Macromolecular Rapid Communications
www.mrc-journal.de

Granular Cellulose Nanofibril Hydrogel Scaffolds for 3D Cell Cultivation

*David B. Gehlen, Niklas Jürgens, Abdolrahman Omidinia-Anarkoli, Tamás Haraszti, Julian George, Andreas Walther, Hua Ye, and Laura De Laporte**

The replacement of diseased and damaged organs remains an challenge in modern medicine. However, through the use of tissue engineering techniques, it may soon be possible to (re)generate tissues and organs using artificial scaffolds. For example, hydrogel networks made from hydrophilic precursor solutions can replicate many properties found in the natural extracellular matrix (ECM) but often lack the dynamic nature of the ECM, as many covalently crosslinked hydrogels possess elastic and static networks with nanoscale pores hindering cell migration without being degradable. To overcome this, macroporous colloidal hydrogels can be prepared to facilitate cell infiltration. Here, an easy method is presented to fabricate granular cellulose nanofibril hydrogel (CNF) scaffolds as porous networks for 3D cell cultivation. CNF is an abundant natural and highly biocompatible material that supports cell adhesion. Granular CNF scaffolds are generated by pre-crosslinking CNF using calcium and subsequently pressing the gel through micrometer-sized nylon meshes. The granular solution is mixed with fibroblasts and crosslinked with cell culture medium. The obtained granular CNF scaffold is significantly softer and enables well-distributed fibroblast growth. This cost-effective material combined with this efficient and facile fabrication technique allows for 3D cell cultivation in an upscalable manner.

Organ failure and loss due to injury or disease remain one of the main challenges to be overcome in modern medicine, with organ donor shortage leading to the death of many patients. The development of synthetic materials that facilitate (re)generation of functional organs has gained considerable interest over the past decades.[1] In tissue engineering, biomaterial scaffolds are engineered to mimic aspects of the native extracellular matrix (ECM). For this purpose, hydrogel scaffolds are water-containing hydrophilic polymer networks that can be tailored to have similar mechanical properties to the ECM, as described in detail elsewhere.[2–4] They are fabricated by crosslinking natural or synthetic polymers and can be formed as a hybrid of both synthetic and natural compounds. Natural polymers have the advantage of resembling the native ECM with inherent bioactivity,[5] while synthetic polymers allow high controllability of the individual properties of the hydrogel, including biofunctionalization and stiffness.[6] However, the success of hydrogel scaffolds is limited by low levels of cell infiltration due to the lack of micron-scale porosity and mismatch with ECM-like dynamic structural properties. Though the native ECM is a dynamic viscoelastic network permissive to cellular remodeling, most conventional synthetic hydrogels consist of an elastic network that acts as a boundary for cells when being nanoporous, inhibiting 3D cell spreading and migration if the material does not degrade.

D. B. Gehlen, N. Jürgens, A. Omidinia-Anarkoli, Dr. T. Haraszti, Prof. L. De Laporte
DWI–Leibniz-Institute for Interactive Materials
Forckenbeckstr. 50 D-52074, Aachen, Germany
E-mail: delaporte@dwi.rwth-aachen.de

D. B. Gehlen, N. Jürgens, A. Omidinia-Anarkoli, Dr. T. Haraszti, Prof. L. De Laporte
Institute for Technical and Macromolecular Chemistry
RWTH Aachen University
Worringerweg 1-2 D-52074, Aachen, Germany

The ORCID identification number(s) for the author(s) of this article can be found under https://doi.org/10.1002/marc.202000191.

DOI: 10.1002/marc.202000191

Dr. J. George, Prof. H. Ye
Institute of Biomedical Engineering
Department of Engineering Science
Old Road Campus Research Building
University of Oxford
Headington OX3 7DQ, Oxford, UK

Prof. A. Walther
Freiburg Center for Interactive Materials and Bioinspired Technologies (FIT)
University of Freiburg
Georges-Köhler-Allee 105 D-79110, Freiburg, Germany

Prof. L. De Laporte
Department of Advanced Materials for Biomedicine
Institute of Applied Medical Engineering
RWTH Aachen University
52074, Aachen, Germany

To overcome the challenges associated with low levels of cell infiltration, most synthetic hydrogels have been designed with degradable groups between the crosslinks. Degradation of these groups weakens the internal scaffold network, permitting proliferation of encapsulated cells inside the hydrogel. Degradation can be achieved either via hydrolysis (ester bonds)[7] or cell mediated via matrix-metalloproteinase (MMP)-sensitive sites.[8] However, in the case of nanoporous networks, it remains difficult to optimize the rate of hydrogel degradation, which is required for cell migration while maintaining sufficient structural integrity and mechanical support during tissue regeneration. Consequently, alternative approaches that increase cell migration are being investigated, for example, through the generation of a greater number of dynamic (breakable) hydrogel backbones or the fabrication of hydrogel scaffolds with increased porosity.

One approach is to exchange nanoporous elastic covalent crosslinks in the hydrogel polymer network with supramolecular or dynamic covalent bonds. The resulting viscoelastic network can be directly remodeled by cellular forces depending on many other factors, such as the spatial organization of cell adhesive domains.[9] As a result, the network does not impede cells with a spring-like resistance but instead provides mechanical support while being permissive to cell growth and migration, likely due to enhanced integrin clustering.[9] Here, porosity and adhesion sites play an important role in efficient cell spreading, mobility, and migration. Alternatively, a combination of degradable and nondegradable crosslinking groups within a hydrogel network results in a partially degradable scaffold, which leads to increased porosity.[10] However, controlling this porosity is limited to changing the ratios of the crosslinking groups, which affects mechanical stability. A number of other approaches have also been developed, including the generation of microporous hydrogels through the use of phase separation during the crosslinking of poly(ethylene glycol) in the presence of highly viscous polysaccharides under physiological conditions,[11] incorporation of biocompatible porogen beads resulting in void forming hydrogels,[12] colloidal-crystal templating techniques,[13] or enzymatic assembly of spherical microgels.[14–19] Spherical microgels can be functionalized with fibrin-derived peptides, allowing for subsequent enzymatic crosslinking between them. Alternatively, physically assembled microgels can be crosslinked through exposure to UV light[20] and microgels can also be assembled by harnessing dynamic ionic interactions.[21]

Unfortunately, most approaches to creating porous structures within hydrogel scaffolds require advanced fabrication techniques and technologies that are relatively expensive and time consuming to perform. Consequently, it is usually only feasible to produce scaffolds in small quantities. In this report, a rapid method is demonstrated to create granular hydrogel systems that support 3D cell growth within cost-effective TEMPO-oxidized cellulose nanofibril (CNF) hydrogels, focusing on upscalability and potential automation instead of complete control over the structure. Cellulose can be derived in abundant quantities from plant or bacterial sources, possesses shear-thinning properties, and can be readily crosslinked via carboxyl groups using glutaraldehyde or calcium ions. The double positively charged calcium ions interact with the negatively charged carboxyl groups of the CNF under physiological conditions. Furthermore, it is biocompatible and supports cell adherence and spreading without further biomodifications. Bioactive gyroid scaffolds have been fabricated by 3D printing sacrificial negative templates, filling the template voids with CNF and subsequently dissolving the templates using a sodium hydroxide solution.[22] As a result, a scaffold with a minimal surface area was generated with internal porosity that facilitated cell growth. Here, the CNF scaffolds maintain shape memory after drying, enabling their placement inside a specific site of injury, after which the scaffold can swell and fill the lesion area. Additionally, using double charged ions or counterions with different sizes allows for manipulation of the mechanical properties of CNF hydrogels, as described in detail elsewhere.[23] The shear-thinning properties of CNF facilitate a variety of processing techniques such as extrusion to produce CNF tubes. For example, freestanding tubular cell constructs can be created by seeding the inner lumen of extruded CNF tubes with fibroblasts, growing a confluent cell layer and then using sequential enzymatic degradation with cellulase to remove the CNF scaffold.[24] Cellulase degradation of CNF hydrogels can also be enhanced in 3D cell culture under specific flow conditions, leading to increased cell proliferation and migration.[25] Drug delivery systems, such as hollow microgels,[26] can be potentially loaded with cellulase to locally degrade the hydrogel. Importantly, one needs to take into account that the lower pH caused by cellular acid production within CNF hydrogels can significantly increase the rate of cellulase enzymatic degradation.[24] In this report, enzymatic degradation is not required to facilitate 3D cell growth in the CNF hydrogel because the granular nature of the generated scaffolds already provides a suitable irregularly fused microporous structure. Granular hydrogels are realized via the crushing of pre-crosslinked CNF through a defined micrometer-sized nylon mesh, after which the crushed CNF is crosslinked by immersion in salt containing medium. The resulting gels fuse irregularly, possess a lower stiffness, and facilitate fibroblasts to spread and interconnect with each other, allowing for the first time the use of CNF for 3D cell growth in a very effective and potential upscalable manner for a variety of applications without the need for cellulase.

To improve the properties of CNF hydrogels for 3D cell culture and tissue formation, a simple approach is established to create granular CNF hydrogels that promote 3D spreading of encapsulated cells (**Figure 1**). CNF is pre-crosslinked in a calcium solution of 2×10^{-3} M and subsequently crushed through a 10 μm pore diameter nylon mesh (Figure S1, Supporting Information). Alternatively, the CNF is pre-crosslinked using 5×10^{-3} M of calcium and crushed through a nylon mesh with larger 41 μm diameter pores. The crushed CNF is mixed with cells and subsequently crosslinked by immersion into cell culture medium. As this medium contains salts, the granular scaffold is crosslinked in a secondary manner into a microporous granular network.

The concentration of calcium for pre-crosslinking the CNF is optimized to achieve the maximal degree of (pre-) crosslinking while still allowing the gel to be crushed through

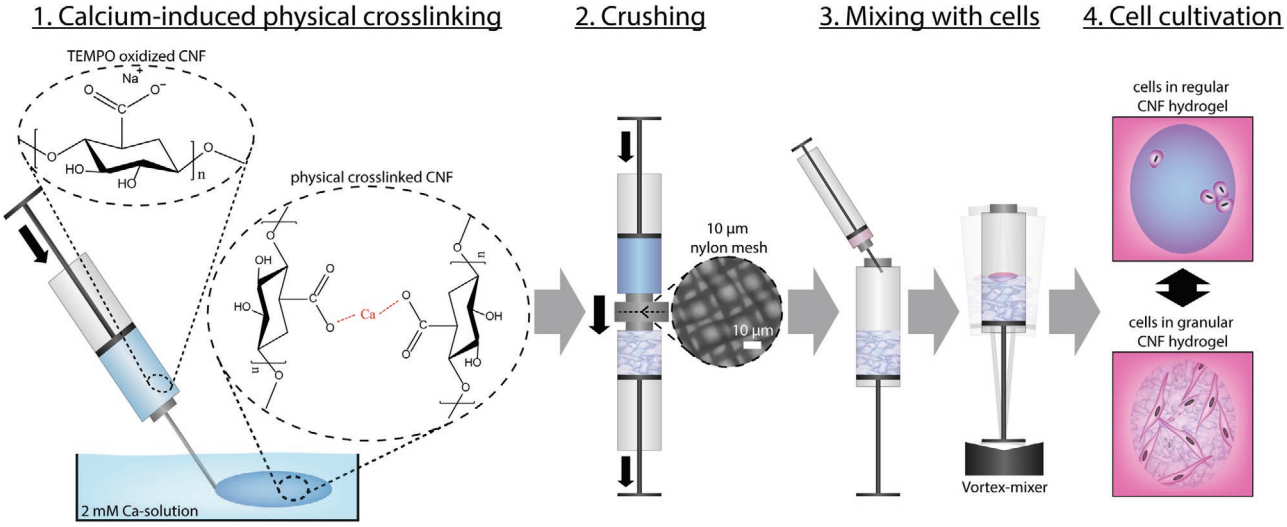

Figure 1. Schematic of the preparation of the granular CNF hydrogel by pre-crosslinking CNF in a 2×10^{-3} M calcium solution, crushing the pre-crosslinked CNF through a nylon mesh and subsequently mixing it with fibroblasts (L929) in medium.

the nylon mesh. In the case of a 10 µm pore diameter mesh, calcium concentrations above 2×10^{-3} M are found to result in crosslinking between the carboxyl groups that renders the gel too stable to press through the mesh. Optimization of the calcium concentration for the 41 µm pore diameter nylon mesh revealed that a higher maximal calcium concentration of 5×10^{-3} M could be used. Rheology measurements are performed at 1.0 Hz frequency and 0.5% strain to analyze the mechanical properties of the granular hydrogels obtained from pre-crosslinking, crushing and subsequent secondary crosslinking between CNF granules by immersion in cell culture medium for a long time of 1 h. CNF, which is directly crosslinked by immersion into cell culture medium (regular) is compared with CNF pre-crosslinked with a 2×10^{-3} M calcium solution, crushed once (single-crush) or multiple times (multicrush) through a 10 µm pore diameter nylon mesh and then crosslinked a second time by immersion into cell culture medium (**Figure 2**A). CNF crosslinked directly with cell culture medium results in a hydrogel with a storage modulus of 2.8 ± 0.3 kPa. The bulk storage modulus of granular CNF hydrogels is found to be significantly reduced, at 980 Pa ± 95 Pa (single-crush) and 746 Pa ± 45 Pa (multicrush). Crushing the CNF multiple times may result in a further reduction of granular hydrogel storage modulus. However, the degree of reduction is found to be statistically insignificant in this investigation. Additionally, the crosslinking of the CNF granules via media incubation resulted in similar storage moduli when the incubation was very short (≈30 s) compared to 1 h, indicating that the calcium-mediated crosslinking reaction is very rapid and occurs almost instantaneously (Figure S2, Supporting Information). To analyze the viscoelastic properties of the single crushed CNF sample, a frequency and amplitude sweep was performed, showing an elastic behavior for the single crushed CNF hydrogel (Figure S3, Supporting Information).

After crushing, 900 µL of the granular CNF hydrogel was mixed by brief vortexing with 100 µL of Roswell Park Memorial Institute 1640 medium supplemented with 10 vol% fetal bovine serum (Biowest) and 1 vol% Gibco antibiotic–antimycotic (RPMI+) containing a high concentration of fibroblasts (L929). Samples of the gel and cell mix (250 µL) are deposited into wells and 1 mL of culture medium is added to each well for crosslinking of the construct. To test whether mixing with cells affected the shear-thinning properties of CNF, the same small amount of cell culture medium (10 vol%) is mixed into both bulk CNF and granular CNF hydrogels. For all conditions, regular versus granular CNF, with and without 10 vol% cell culture medium (equivalent to the volume used when adding cells), the storage and loss moduli are measured with alternating stress rates of 0.5% and 500% at 1.0 Hz (Figure 2B–E), revealing that the shear-thinning properties of CNF hydrogels are maintained in the presence of 10 vol% medium, and that a single crush did not change this. Overall, the storage modulus increases only slightly due to the addition of salt-containing culture medium (10 vol%). Immersion of the granular CNF into a large volume of RPMI+ medium leads to complete crosslinking and loss of the shear-thinning properties, making it impossible to pipette.

Fibroblasts mixed into the granular CNF hydrogels are cultivated alongside control cultures of fibroblasts mixed directly into noncrushed CNF hydrogels. After 7 days of culture, cell spreading and morphology are compared between the different scaffolds by cytoskeleton staining for F-actin using Phalloidin-488 (**Figure 3**). While cells do not spread and grow when mixed directly into CNF, the granular CNF hydrogels are found to support cellular spreading and distribution in 3D (Videos S1–S5, Supporting Information). Interestingly, the cells are found to be more uniformly distributed throughout the single-crushed granular CNF scaffolds in comparison to the multicrushed granular CNF scaffolds. It may be that crushing the CNF multiple times leads to reduced overall integrity of the bulk granular network, resulting in a more heterogeneous internal structure, containing areas with different amounts of cell growth. This is in agreement with the bubble/void formation, observed after the multiple crushing steps, and the increase in opacity

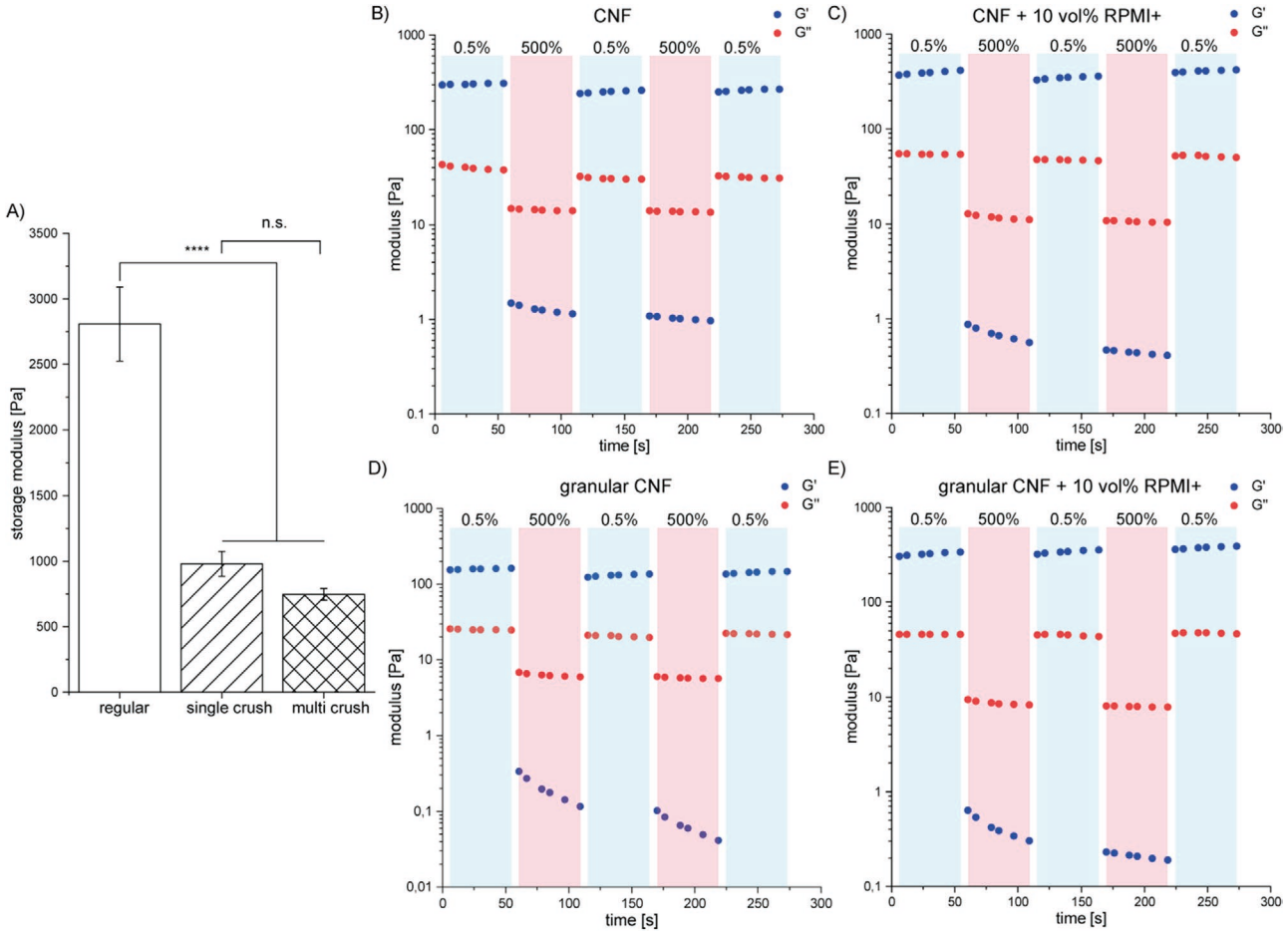

Figure 2. A) Rheology measurements of CNF hydrogels immediately crosslinked by full immersion in cell culture RPMI+ medium for 1 h, CNF pre-crosslinked in a calcium solution of 2×10^{-3} M and subsequently crushed once (single-crush) before crosslinking in medium, and pre-crosslinked CNF crushed multiple times (multi crush) through a 10 µm nylon mesh before crosslinking in medium for 1 h. The moduli reveal a reduction in stiffness for the granular CNF hydrogels obtained by the crosslinking–crushing–crosslinking process. B–E) Shear-thinning properties of nongranular, non-crosslinked CNF hydrogels, nongranular CNF with 10 vol% RPMI+, and granular CNF hydrogels without or with 10 vol% of RPMI+ medium (equivalent to the volume used when adding cells). $n \geq 4$ and error bars representing standard deviations for (A).

(Figure S4, Supporting Information). Granular CNF hydrogels generated with 10 and 41 µm pore diameter nylon mesh reveal similar trends for single versus multicrushing and comparable cell growth for single crushed gels. In the case of multicrushing, the granular gel fabricated using the 41 µm pore diameter nylon mesh results in decreased cell spreading and growth in comparison to granular gels fabricated using the 10 µm pore diameter nylon mesh.

To analyze 3D cell growth and quantify the distribution of the cells in the hydrogel-scaffold, all layers of the z-stacks of at least three samples are quantified by dividing them into 100 sectors. For each sector, the amount of F-actin signal is calculated. Subsequently, the amount of summed F-actin signal in each sector is normalized by the average (normalized voxel count) to reflect how evenly distributed the cells are located inside the different CNF hydrogels.

Normalized voxel counts of 1 equate to a sector with as many cells as the average cell amount per sector, whereas voxel counts closer to 0 represent sectors with very few cells and sectors with high voxel numbers represent densely populated areas containing higher cell numbers and cell aggregates. For example, hydrogel constructs containing homogeneously distributed cells will have many sectors with normalized voxel counts around 1, whereas CNF hydrogels with inhomogeneous cell distributions will mainly have sectors with normalized voxel counts tending toward zero or very high values and only a few sectors close to 1. An inhomogeneous distribution is observed for cells mixed directly in CNF, whereas cell density is found to be more uniform throughout granular CNF scaffolds multicrushed through a 10 µm pore diameter mesh and very well distributed (showing a clear maximum around 1) in the case of CNF scaffolds single-crushed through 10 µm pore diameter mesh (**Figure 4**). Quantification of the distribution in the CNF scaffolds crushed through 41 µm pore diameter mesh reveals the same difference between the single and multiple crushed granular gels with less homogeneous cell distribution in multicrushed samples. Furthermore, cell distribution throughout the 10 µm pore diameter mesh granular gel is more uniform when compared with the 41 µm pore diameter mesh granular gel. Overall, quantification of cell distribution shows that the

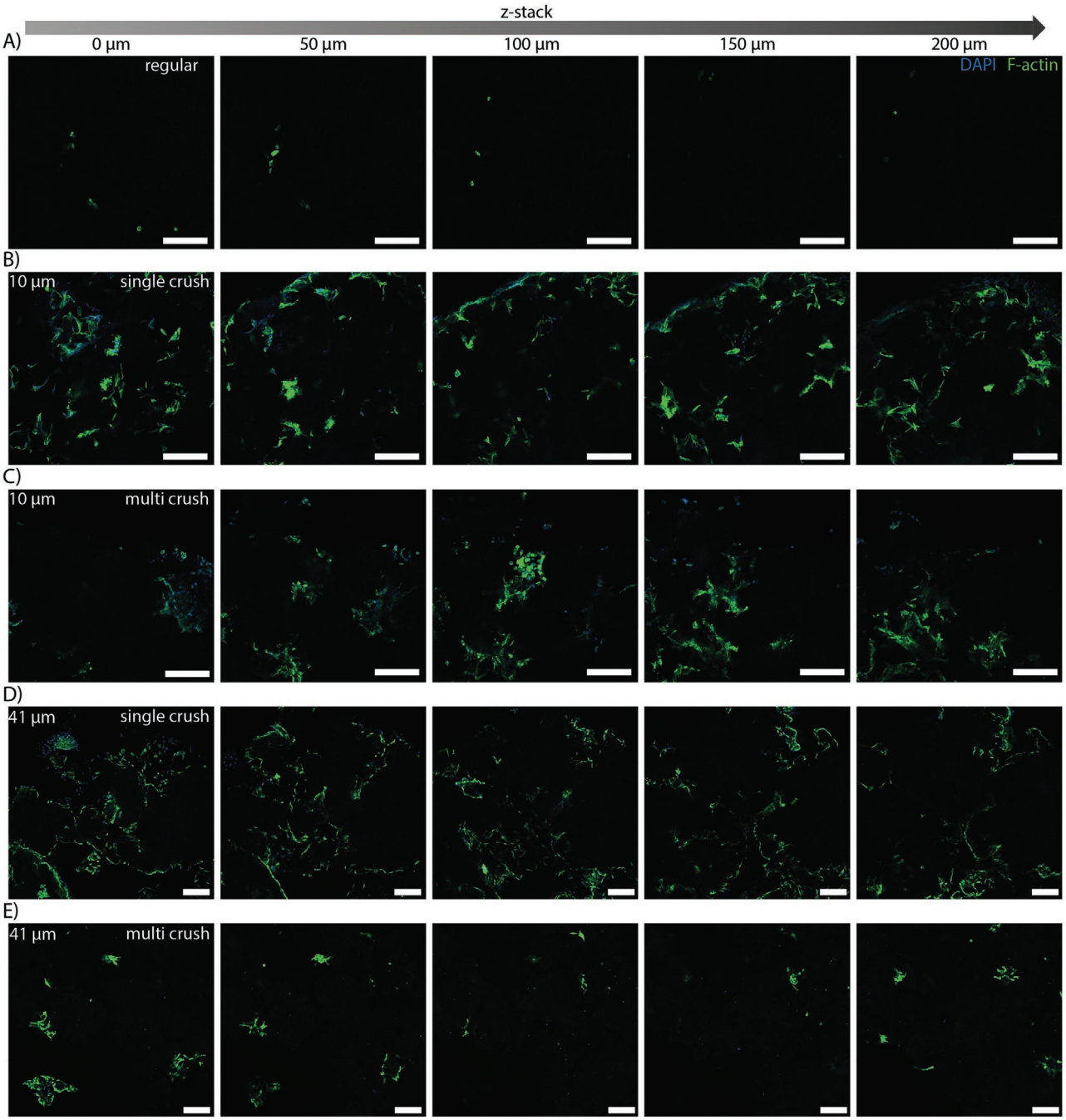

Figure 3. z-Stack images (50 µm distance between each image) of fibroblasts (F-actin skeleton in green and DAPI in blue) mixed directly in CNF A), and in granular CNF scaffolds, which are crushed once B) or multiple times C) through a 10 µm pore diameter nylon mesh, or once D) or multiple times E) through a 41 µm pore diameter nylon mesh after 7 days of culture. The fibroblasts inside the granular CNF scaffolds are better distributed and have a greater spread morphology over the entire z-stack, indicating improved 3D growth of the cells in these conditions. Scale bars represent 200 µm. For videos of z-scans, see Videos S1–S5 in the Supporting Information.

cells are better distributed in granular CNF hydrogels fabricated by single crushing though 10 µm pore diameter nylon mesh.

To further quantify the difference of the distributions, a cross-comparison matrix containing a two-sided Kolmogorov–Smirnov test is generated for the normalized voxel counts of all individual samples (Figure S5, Supporting Information). This enables us analyzing whether two data sets are coming from a similar ensemble (cell distribution inside hydrogel) based on their integral distribution. Very low p values allow for rejecting this hypothesis, thus revealing that two ensembles are significantly different. The results show clearly that the regular CNF is different from all crushed CNF conditions ($p < 0.001$, marked in gray). Additionally, overall differences between 10 and 41 µm and single and multiple crushed samples are observed, even

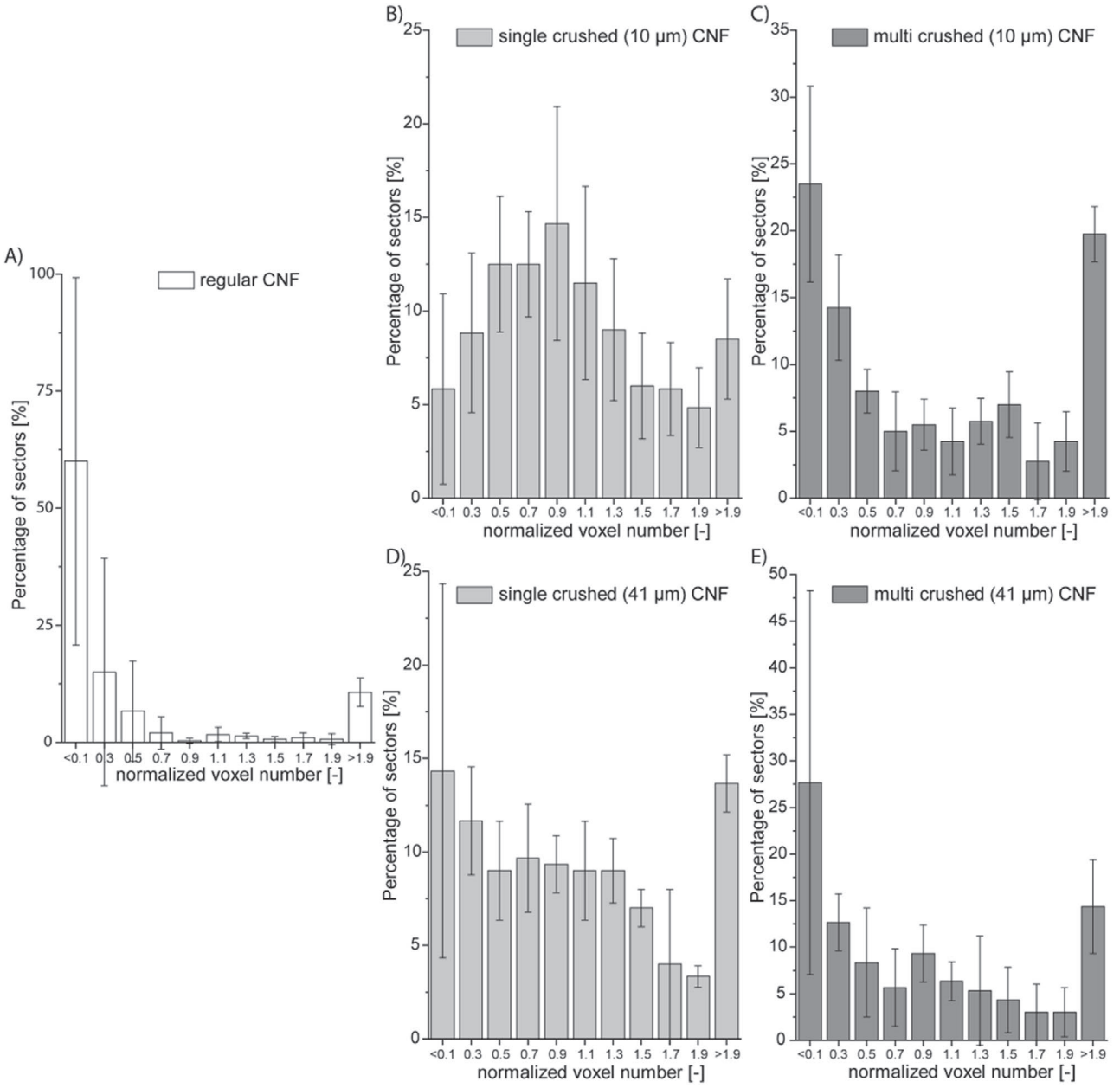

Figure 4. Quantification of cell distribution (F-actin signal) revealing an inhomogeneous cell distribution in regular CNF (A), whereas a more uniform centrally focused cell distribution is found in single crushed CNF hydrogels for gels crushed through both 10 µm (B) and 41 µm (D) pore diameter meshes. Cell distributions in CNF granular gels crushing multiple times through 10 µm (C) or 41 µm (E) pore diameter meshes are less uniform than single-crushed granular CNF gel but more uniform than bulk CNF gel. $n \geq 3$ and error bars representing standard deviations.

though for some of the individual samples of different conditions this hypothesis cannot be clearly rejected. This shows that when comparing the mesh size or number of crushing steps, there is only a tendency for more homogeneous cell distributions when 10 µm nylon meshes and a single crush step are used.

To better visualize cell morphology inside the crushed CNF hydrogel, magnified 3D images of the cells are analyzed for single crushed CNF through 10 µm nylon mesh and compared to regular CNF (Figure S6, Supporting Information). While cells in regular CNF have no space for spreading and are rounded up, the individual cells in the crushed CNF are spreading randomly in all directions without following any visibly structures/orders or filling defined macropores (Videos S6 and S7, Supporting Information).

To gain more insight into the hydrogel internal structures and encapsulated cells, cryogenic scanning electron microscopy (cryo-SEM) is used. This method is particularly advantageous as hydrogel structures can be preserved that would otherwise be lost when drying to perform conventional

SEM. Figure S7 (Supporting Information) demonstrates fully hydrated 3D hydrogels of pure CNF and single crushed CNF hydrogels with and without cells (10 μm nylon mesh). As expected, all hydrogels demonstrate the typical nano/microporous structure of hydrated hydrogels. Even though this was not completely conclusive, the crushed hydrogels exhibit a morphologically different structure, likely due to the treatment process. During CNF hydrogel extrusion through the nylon micromesh, the calcium-crosslinked hydrogel bulk structure undergoes a compression (applied by the syringe plunger against nylon mesh) and shear force (when passing through the nylon mesh). As the CNF hydrogel loses its shear-thinning properties after crosslinking in calcium, it cannot longer form a microscopically uniform hydrogel after extrusion, yet, consists of disrupted internal structures, which is only partially visible (Figure S7B, Supporting Information) but has a large effect on cell growth. Figure S7C (Supporting Information) demonstrates encapsulated cells within the 3D hydrogel matrix supporting the efficiency of the crushing step. As a conclusion, it can be stated that the crushed CNF fused back together to a certain degree but irregularly and not as homogeneous as it was before, allowing cells to spread inside the hydrogel. However, the detailed mechanism of cell-material interaction and the local effect of cell forces on the material requires further studies.

For additional characterization of the hydrogel, diffusion experiments are performed using either high molecular weight fluorescein isocyanate dextran with an average molecular weight of 2000 000 g mol^{-1} or red fluorescent nanoparticles with a size of 100 nm. The solutions are incubated overnight at 37 °C together with calcium crosslinked CNF hydrogels (regular or single or multiple times crushed through 10 μm nylon meshes) to analyze to which extend they diffuse into the hydrogels (Figure S8, Supporting Information). While the dextran molecules completely diffused into all hydrogel samples, which can be explained by the general porosity of CNF hydrogels in the range of 0–60 nm,[22] no 100 nm nanoparticles can penetrate any of the samples, indicating that the potential difference in porosity/structure is below 100 nm. Importantly, the fact that the 100 nm nanoparticles cannot infiltrate into the crushed CNF hydrogel confirms that the crushed CNF fuses back together after crushing, although irregularly, allowing cells to spread homogeneously after a single crush. Comparing the images of the diffused dextran with regular and single crushed CNF shows a slightly different structure, which also indicates the irregular and less stable fusion after crushing. For the multicrushed samples, bubbles/voids are observed, which explain the irregular cell distribution for the multicrushed samples.

After characterizing the irregularly fused structure of the crushed CNF, an important question is whether cells are not only able to spread in 3D when embedded inside the hydrogel but if they are also able to infiltrate the CNF scaffold when seeded on top. Therefore, cells are seeded on top of regular, single, or multiple times crushed (10 μm nylon mesh) CNF hydrogels and bright field images are taken over time (Figures S9–S11, Supporting Information). Confocal microscopy is performed after 7 days of cultivation (Figure S12 and Videos S8–S10, Supporting Information). In general, the cells prefer to grow in a 2D manner on the surface as long as possible, indicating again that the crushed CNF fused irregularly together without creating macropores, in which cells can infiltrate rapidly. Importantly, while cells grow a confluent 2D monolayer after ≈3 days for all conditions, no cell infiltration is observed for regular CNF and only minimal numbers of cells grow into the multi crushed CNF when there is a void/bubble next to the surface. In contrast, partial cell infiltration occurs for the single crushed CNF after 7 days, indicating that the structure of the CNF is weakened and allows cells to spread.

Additional degradation of the CNF by supplementing cellulase to the medium could potentially increase the infiltration of the cells into the CNF hydrogel. Therefore, we added 1 and 2 g L^{-1} cellulase to the medium. However, only a small increase of cell infiltration is observed when supplementing cellulase to the medium, while the CNF hydrogels became very fragile over time due to the degradation, which was more significant in the case of crushed CNF hydrogels. Furthermore, in the cell infiltration studies, supplementing cellulase results in a higher tendency of the 2D growing cells to detach from the surface (Figure S13, Supporting Information). It is known that the presence of cells leads to a decrease in pH, which significantly fastens the degradation activity of the enzyme.[24] Therefore, it is likely that the cells on the surface locally increase the degradation, leading to a loss of contact with the CNF surface and detachment of the cell layer instead of an enhanced infiltration into the CNF hydrogel.

The rapid generation of granular CNF hydrogel constructs using this novel technique is found to be an effective approach for the preparation of cost-effective, biocompatible, and cell-adhesive scaffolds for 3D homogeneous cell growth throughout the entire construct. Even though the creation of these scaffolds is not focused on creating a homogeneous pore structure, like in the case of microgel assembly, as the CNF fuses irregularly back together after crushing, this method allows for potential upscaling and automation. This opens the path for high-throughput screening platforms with better control over the biochemical parameters compared to other 3D hydrogel materials, such as Matrigel. Consequently, the generated granular scaffold is an irregularly fused hydrogel with internal mechanical instability, allowing 3D cell spreading, which is not comparable with regular CNF hydrogels. The described method enhances the potential of using CNF as a 3D scaffold for cell culture and tissue formation, facilitating cell spreading and migration, and decoupling the need for enzymatic degradation by cellulase to provide space, and with mechanical instability to enable cell spreading within the hydrogel. As CNF inherently promotes cell adhesion, no additional biofunctionalization with cell-adhesive peptides or proteins was found to be necessary. The reason for this can be explained by the negatively charged carboxyl groups under physiological conditions, which can interact with positively charged proteins which are important for cell adhesion, such as collagen-1, as previously postulated.[22] Large-scale production of CNF is cost-effective and the reported technique used to generate granular CNF hydrogels can be easily modified for large-scale production. Furthermore, the method is suitable for use in high-throughput

screening platforms that can be used for drug testing. In addition, the convenience of being able to pipette granular hydrogel due to shear-thinning and the ease of secondary crosslinked scaffold assembly makes the granular CNF hydrogel systems suitable for extrusion applications. For example, granular hydrogels are ideal candidate materials for use in bioprinting, facilitating the generation of complex hierarchical structures in a controllable manner.[27–30] Also of interest is the ease in which this approach can be used to combine 3D culture of multiple cell types to grow complex tissues ex vivo, as demonstrated by previous publications.[31] Additionally, the use of granular CNF hydrogel in combination with other factors that control granule degradation rates will enable the technique discussed to be transferred to many existing applications, for example with cellulase-based drug delivery systems[26] and highly customizable controlled flow inside bioreactor systems.[25]

Experimental Section

Preparation of the Granular CNF Hydrogels: The preparation of the CNF hydrogel was described elsewhere.[22] The CNF and all of the equipment were either sterilized by autoclaving or purchased under sterile condition, while all cell experiments were performed under sterile conditions. 3.0 mL of 2×10^{-3} M (or 5×10^{-3} M) calcium chloride (Sigma Aldrich) solution was pipetted on top of a 1.0 mL CNF hydrogel and left for 2 min at room temperature for pre-crosslinking. The calcium chloride solution was subsequently removed and the pre-crosslinked CNF hydrogel was transferred with a spatula to a 2 mL syringe (Braun) by removing the piston and filling the syringe through the back end. Next, a 10 or 41 µm nylon mesh (Merck Millipore Ltd.) was placed into a 3D-resin-printed filter adapter for syringes for the mechanical studies and into an autoclave sterilized metal filter adapter (Merck Millipore Ltd.) for cell experiments. Subsequently, the pre-crosslinked CNF was pressed through the filter to generate granular CNF, which was then used for cell experiments. A syringe was placed at the other side of the adapter to capture the granular CNF hydrogel, allowing it to crush the gel either once or multiple times through the nylon mesh filter (Figure S14, Supporting Information).

Rheology Measurement: The mechanical properties of the samples were determined with a TA Instruments Discovery HR-3 rheometer, equipped with a 20 mm diameter geometry with a cone angle of 2.002°. 74 µL of the regular CNF or the granular CNF, prepared as described before, was placed in the middle of the Peltier-plate with a viscous pipet (Mettler Toledo) and the geometry was lowered to create a measuring gap of 51 µm to press the CNF into the correct shape. Next, 1.5 mL of cell culture medium (RPMI+, Thermo Fisher Scientific) was pipetted around the sample and the geometry was lifted to ensure that the cell culture medium is surrounding the entire CNF. The solution was then covered and left for 1 h for crosslinking or only 10 s (≈30 s of total immersion time of the CNF in RPMI+ medium) for analyzing the speed of calcium crosslinking. Subsequently, the geometry was lowered again to create a measuring gap of 51 µm and the excess cell culture medium was removed with a pipette from around the geometry to enable the measurement. This approach allows for measuring the hydrogel mechanical properties without any drying and a good interface between the hydrogel, Peltier plate, and rheometer geometry. The measurement was performed at 25 °C with a frequency of 1.0 Hz and a strain of 0.5% for a total duration of 5 min. For measuring the shear-thinning properties, 74 µL of regular CNF, CNF mixed with 10 vol% of cell culture medium (RPMI+), and pre-crosslinked (2×10^{-3} M calcium) single crushed (10 µm mesh) CNF without or with 10 vol% RPMI+ was pipetted into the center of the Peltier plate and measured using the 20 mm diameter geometry with a cone angle of 2.002° at 25 °C. The samples were measured with alternating strains of 0.5% and 500% at 1.0 Hz for 60 s per condition and the storage and loss modulus were determined depending on the shear rate.

Cell Experiments: Either 900 µL of regular CNF or granular CNF inside of a 2 mL syringe was mixed with 100 µL of 5000 mouse fibroblast cells μL^{-1} (L929, DSMZ Leibniz Institute) in RPMI+ and mixed gently with the lowest speed on a Vortex mixer (IKA, Vortex 2) resulting in a final density of 500 well-distributed cells μL^{-1} inside the CNF hydrogel. For each sample, 250 µL of the mixture was pipetted into a four-well plate (Thermo Scientific) with a needle (18G, Braun) and crosslinked by adding 1 mL of RPMI+. The samples were cultivated for 7 days at 37 °C and 5 vol% CO_2, while cell culture medium was replaced after 3 days. For analyzing cell infiltration into CNF hydrogels, either ≈150 µL of regular CNF or single or multiple times crushed (10 µm nylon mesh) CNF was pipetted without adding cells on coverslips inside of 48 well plates to cover the entire surface. Subsequently, 500 µL of 50 000 fibroblasts mL^{-1} (L929) was pipetted on top of the CNF hydrogels (total 25 000 cells per well) and incubated for 7 days. Bright field images were taken over time to analyze the growth progress and the coverslips with the CNF hydrogels on top were carefully taken out for confocal microscopy. After 7 days, the cell culture medium was removed and all samples were washed three times with phosphate buffered saline (PBS, 1×, Lonza) for 20 min. The PBS was then replaced with a 4 wt% solution of paraformaldehyde for 1 h for fixation, after which the samples were washed again three times with PBS. The samples were then blocked three times with 4 wt% of bovine serum albumin (BSA, Sigma Aldrich) in PBS for 20 min, and then stained with Phalloidin-iFluor 488 in 4 wt% BSA at 37 °C overnight under the exclusion of light. The samples were sequentially washed three times with PBS and stained with 4′,6-diamidino-2-phenylindole (DAPI, 1:100 in PBS, AppliChem) for 1 h and finally washed again three times with PBS. The samples were stored at 4 °C until imaging using confocal microscopy. Confocal imaging was performed on an SP8 Tandem Confocal (Leica Microsystems Inc.) and bright field images were taken using a Zeiss Axio Observer Z1 microscope. Image processing was performed using LasX-Software, Zeiss-Zen-Software, and ImageJ.

Quantification: For quantification of the cell distribution inside of the CNF hydrogel constructs, the distributions of the F-actin signal (Phalloidin-iFluor 488) of the confocal images of at least three samples were analyzed ($n \geq 3$). The z-stacks were manually converted into binary images and an overlay is fitted to the image with 10×10 squares. The depth of each sector was chosen as the full depth of the stack and the number of voxels above threshold in each of the 100 sectors was counted using the ImageJ plugin "Voxel Counter" for at least three samples. The counted amount of all z-stacks per sector was summed and subsequently divided by the average for normalization. It is defined as normalized voxel numbers. Next, a histogram with the percentage of sectors (N) with specific normalized voxel numbers was calculated with 0.2 intervals between 0.1 and 1.9, as well as values below 0.1 or above 1.9. For each sector, the average and standard deviation of at least three samples for the histograms were determined. Many values equal or close to 1 represent a homogeneous distribution in all sectors, whereas many empty (>0.1) and highly packed (<1.9) sectors represent heterogeneous distributions within the sample. To further quantify the difference between two distributions, a two-sided Kolmogorov–Smirnov test was performed on the normalized voxel count values. To compare the p values for all individual samples, a cross-comparison matrix was built. The calculations were performed using R (Copyright 2020 The R Foundation for Statistical Computing). Values below 10^{-12} are marked as 0 and the lower half under the diagonal of the matrix is not tested due to the symmetry. To investigate the strength of a two-sided Kolmogorov–Smirnov test for this data setup, a model was designed, assuming homogeneous mixing of cells inside a hydrogel, which are assumed to produce average amounts of actin fibers. Due to cell behavior, staining, and signal noise, different distributions will occur. Overall, it was assumed that the 10×10 grid resulted in a voxel count per sector (I), which obeys a normal distribution built up from three factors: the number of cells in the sample, the amount of F-actin in a cell, which is related to the cell size, and the efficiency of the staining. This normal

distribution was characterized by a mean value 1000 (chosen arbitrarily to be similar to the experimental data) and a standard deviation (s.d.) σ (100, 200, 500, and 1000). As in this model, negative value would be associated with death of all cells, the values in these sectors were set to zero. First, three samples were generated with the lowest s.d. value (σ = 100) to test how the method works for samples drawn from the same ensemble. After that, the first sample of these three was compared to higher s.d. showing lower p values. For an s.d. equal to or above 500, p values below 0.001 were observed. Each model sample image was treated the same way as the data in Figure 4. Normalization via the mean I_0 of all sectors changes the mean value of a standard distribution to 1 with a rescaled standard deviation of σ/I_0. This leads to a distribution of the percentage of sectors in the form

$$N = 100 \cdot e^{\frac{-\left(\frac{I}{I_0}-1\right)^2}{2\left(\frac{\sigma}{I_0}\right)^2}} \quad (1)$$

Additionally, the distributions show the expected tendency to have a maximum around 1 for small standard deviations and maxima around 0 and high values (1.9 or higher) for increasing standard deviations (Figure S15, Supporting Information). Performing the two-sided Kolmogorov–Smirnov test for these simulated distributions with different standard deviations demonstrated that the p values represent the differences in the histograms (very small values, typically under 10^{-3} to reject the hypothesis).

Cryogenic Scanning Electron Microscopy (cryo-SEM): For high-resolution analysis of the structure with cryo-SEM, the CNF hydrogels were placed on a sample holder, frozen in liquid ethane for 1 min, and transferred into liquid nitrogen. Cross-sections of the samples were cut inside the prechamber and were visualized at 3 kV and 2.3 µA for gel only samples and at 1.5 kV and 2.3 µA for gel samples with cells using the field emission scanning electron microscope SU4800 (Hitachi Ltd. Corporation) after sublimation for 5–15 min up to –80 °C.

Diffusion Experiment: For further analysis of the inner structure of the CNF hydrogels, diffusion experiments were performed using high molecular weight fluorescein isocyanate dextran with an average molecular weight of 2000 000 g mol^{-1} (Sigma Aldrich) or red fluorescent nanoparticles with a size of 100 nm (FluoSpheres carboxylate-modified microspheres, Invitrogen, F8801) kindly provided by Prof. Rudolf Merkel (Forschungszentrum Juelich). Regular CNF hydrogels or single or multiple times crushed CNF hydrogels through a 10 µm nylon mesh were prepared as described above with the difference that 30 µL was immersed inside of 200 µL of a 100 × 10^{-3} M calcium chloride solution instead of cell culture media to avoid autofluorescence. After 1 h incubation at room temperature, the calcium solution was replaced by 100 µL of a 100 × 10^{-3} M calcium solution supplemented with either 1 g L^{-1} dextran or 1 vol% of the fluorescent bead solution. The samples were then incubated overnight at 37 °C and taken out of the dye-solutions into fresh 100 × 10^{-3} M calcium solution without dye for analysis at the confocal microscope.

Statistics: General statistical analysis was performed using OriginPro 2018b. A one-way analysis of variance was performed with Bonferroni and Tukey comparisons to determine statistical significance. Data points were depicted as mean average with error bars indicating the standard deviation. The p values for statistical significance are represented with stars: *p < 0.05, **p < 0.01, ***p < 0.001, and ****p < 0.0001. Statistical analysis via Kolmogorov–Smirnov test was performed as described in the Quantification section.

Supporting Information

Supporting Information is available from the Wiley Online Library or from the author.

Acknowledgements

The authors thank Frederik Stolz for solving general laboratory workflow issues, and Dr. Nora Wallot-Hieke and Dr. Jose Luis Gerardo Nava for helping with processing the z-stack images. The authors also acknowledge the European Commission (EUSMI, 731019), the European Research Council (ERC) under the European Union's Horizon 2020 research and innovation program (ANISOGEL, Grant agreement No. 637853), and China Regenerative Medicine International Ltd. This work was partially performed at the Center for Chemical Polymer Technology (CPT), which was supported by the EU and the federal state of North Rhine Westphalia (Grant No. EFRE 300088302).

Open access funding enabled and organized by Projekt DEAL.

Conflict of Interest

The authors declare no conflict of interest.

Keywords

3D cell cultures, cellulose nanofibril hydrogels, granular hydrogel scaffolds, tissue engineering

Received: April 7, 2020
Revised: July 6, 2020
Published online: August 11, 2020

[1] J. C. Rose, L. De Laporte, *Adv. Healthcare Mater.* **2018**, *7*, 1701067.
[2] K. Y. Lee, D. J. Mooney, *Chem. Rev.* **2001**, *101*, 1869.
[3] M. Lutolf, J. Hubbell, *Nat. Biotechnol.* **2005**, *23*, 47.
[4] D. Seliktar, *Science* **2012**, *336*, 1124.
[5] D. A. Gyles, L. D. Castro, J. O. C. SilvaJr, R. M. Ribeiro-Costa, *Eur. Polym. J.* **2017**, *88*, 373.
[6] C. Licht, J. C. Rose, A. O. Anarkoli, D. Blondel, M. Roccio, T. Haraszti, D. B. Gehlen, J. A. Hubbell, M. P. Lutolf, L. De Laporte, *Biomacromolecules* **2019**, *20*, 4075.
[7] Y. S. Jo, J. Gantz, J. A. Hubbell, M. P. Lutolf, *Soft Matter* **2009**, *5*, 440.
[8] J. Patterson, J. A. Hubbell, *Biomaterials* **2010**, *31*, 7836.
[9] O. Chaudhuri, L. Gu, D. Klumpers, M. Darnell, S. A. Bencherif, J. C. Weaver, N. Huebsch, H. -P. Lee, E. Lippens, G. N. Duda, *Nat. Mater.* **2016**, *15*, 326.
[10] N. Gjorevski, N. Sachs, A. Manfrin, S. Giger, M. E. Bragina, P. Ordóñez-Morán, H. Clevers, M. P. Lutolf, *Nature* **2016**, *539*, 560.
[11] N. Broguiere, A. Husch, G. Palazzolo, F. Bradke, S. Madduri, M. Zenobi-Wong, *Biomaterials* **2019**, *200*, 56.
[12] N. Huebsch, E. Lippens, K. Lee, M. Mehta, S. T. Koshy, M. C. Darnell, R. M. Desai, C. M. Madl, M. Xu, X. Zhao, *Nat. Mater.* **2015**, *14*, 1269.
[13] A. N. Stachowiak, A. Bershteyn, E. Tzatzalos, D. J. Irvine, *Adv. Mater.* **2005**, *17*, 399.
[14] N. J. Darling, E. Sideris, N. Hamada, S. T. Carmichael, T. Segura, *Adv. Sci.* **2018**, *5*, 1801046.
[15] L. R. Nih, E. Sideris, S. T. Carmichael, T. Segura, *Adv. Mater.* **2017**, *29*, 1606471.
[16] N. F. Truong, E. Kurt, N. Tahmizyan, S. C. Lesher-Pérez, M. Chen, N. J. Darling, W. Xi, T. Segura, *Acta Biomater.* **2019**, *94*, 160.
[17] D. R. Griffin, W. M. Weaver, P. O. Scumpia, D. Di Carlo, T. Segura, *Nat. Mater.* **2015**, *14*, 737.
[18] J. Koh, D. R. Griffin, M. M. Archang, A. C. Feng, T. Horn, M. Margolis, D. Zalazar, T. Segura, P. O. Scumpia, D. Di Carlo, *Small* **2019**, *15*, 1903147.

[19] S. Hou, R. Lake, S. Park, S. Edwards, C. Jones, K. J. Jeong, *ACS Appl. Bio Mater.* **2018**, *1*, 1430.
[20] A. Sheikhi, J. de Rutte, R. Haghniaz, O. Akouissi, A. Sohrabi, D. Di Carlo, A. Khademhosseini, *Biomaterials* **2019**, *192*, 560.
[21] S. Wu, M. Zhu, D. Lu, A. H. Milani, Q. Lian, L. A. Fielding, B. R. Saunders, M. J. Derry, S. P. Armes, D. Adlam, *Chem. Sci.* **2019**, *10*, 8832.
[22] J. G. Torres-Rendon, T. Femmer, L. De Laporte, T. Tigges, K. Rahimi, F. Gremse, S. Zafarnia, W. Lederle, S. Ifuku, M. Wessling, *Adv. Mater.* **2015**, *27*, 2989.
[23] A. J. Benítez, A. Walther, *Biomacromolecules* **2017**, *18*, 1642.
[24] J. G. Torres-Rendon, M. Köpf, D. Gehlen, A. Blaeser, H. Fischer, L. D. Laporte, A. Walther, *Biomacromolecules* **2016**, *17*, 905.
[25] M. Krüger, B. Spee, A. Walther, L. De Laporte, L. M. Kock, ASME *J. Med. Diagn.* **2019**, *2*, 041001.
[26] L. P. Guerzoni, J. Bohl, A. Jans, J. C. Rose, J. Koehler, A. J. Kuehne, L. De Laporte, *Biomater. Sci.* **2017**, *5*, 1549.
[27] O. Jeon, Y. B. Lee, T. Hinton, A. Feinberg, E. Alsberg, *Mater. Today Chem.* **2019**, *12*, 61.
[28] S. Xin, D. Chimene, J. E. Garza, A. K. Gaharwar, D. L. Alge, *Biomater. Sci.* **2019**, *7*, 1179.
[29] M. Shin, K. H. Song, J. C. Burrell, D. K. Cullen, J. A. Burdick, *Adv. Sci.* **2019**, *6*, 1901229.
[30] C. B. Highley, K. H. Song, A. C. Daly, J. A. Burdick, *Adv. Sci.* **2019**, *6*, 1801076.
[31] L. P. Guerzoni, J. C. Rose, D. B. Gehlen, A. Jans, T. Haraszti, M. Wessling, A. J. Kuehne, L. De Laporte, *Small* **2019**, *15*, 1900692.